Int. Journal of Refractory Metals and Hard Materials 42 (2014) 163–168

Contents lists available at ScienceDirect

Int. Journal of Refractory Metals and Hard Materials

journal homepage: www.elsevier.com/locate/IJRMHM

Fatigue testing and microstructural characterization of tungsten heavy alloy Densimet 185

M. Pasalic [a], F. Rustempasic [a], S. Iyengar [a,*], S. Melin [b], E. Noah [c]

[a] Materials Engineering, Lund University, 22100 Lund, Sweden
[b] Mechanics, Lund University, 22100 Lund, Sweden
[c] European Spallation Source, Lund, Sweden

ARTICLE INFO

Article history:
Received 1 July 2013
Accepted 4 September 2013

Keywords:
Tungsten heavy alloy
Spallation target
Fatigue life
Microstructure

ABSTRACT

A rotating target consisting of helium-cooled tungsten has been chosen for the European Spallation Source (ESS) facility to be built in Lund. Thermo-mechanical cycling due to the incidence of the proton beam every 2 s on any given tungsten slab in the rotating wheel could lead to crack formation and failure over the lifetime of the target. This work reports tensile and fatigue data obtained at room temperature for the Densimet 185 alloy in the non-irradiated condition. Methods for extracting relevant parameters from fatigue curves with small sets of data are discussed. Fatigue results show a large spread of data for which the application of such methods is challenging. Stress controlled fatigue testing was carried out in this study with mean stress approaching zero and amplitudes in the range 250 to 450 MPa, with 50 MPa increments. A frequency of 25Hz was employed and the fatigue tests lasted until failure was registered or until the upper limit of 2×10^6 cycles was reached. No failure due to fatigue occurred in specimens subjected to stress amplitudes below 300 MPa. Microstructural and fractographic studies on the fatigue samples using Scanning Electron Microscopy (SEM) and Energy Dispersive Spectroscopy (EDS) showed that the samples had low porosity, large and nearly spherical tungsten grains, and with a fairly uniform distribution of the ductile phase rich in nickel and iron. However, bonding between tungsten grains in some areas was found to be inadequate. Intergranular fracture was predominant in the specimens at room temperature. Data for the D185 alloy are compared to those for IT180 and D176 alloys obtained in a previous study and strategies for improving the fatigue strength are discussed.

1. Introduction

Characterization of materials using light/electron microscopy as well as X-ray diffraction is well established and used as a standard procedure for examining materials. However, the use of neutrons in materials research is still not widespread although its usefulness and advantages over conventional methods are now well recognized. In this context, it is interesting to note the setting up of a neutron facility at the European Spallation Source (ESS) site in Lund. This facility can be likened to a gigantic microscope that uses neutrons instead of light to examine materials. Tungsten alloys were initially considered as potential target materials in this facility and this paper examines the suitability of tungsten heavy alloy Densimet 185 (W–2 wt.% Ni–1 wt.% Fe), primarily from a fatigue viewpoint.

The pulsing of the proton beam during the spallation procedure results in rapid changes in temperature and thermal expansion or shrinkage, leading to stresses in the material. It is therefore necessary to cool the target material effectively in order to minimize thermal stresses. In this context, rotation of the target is beneficial and needs to be optimized to maximize the time between beam pulses impinging on the same region of the target. Limiting the increase in target temperature to a minimum is desirable in order to minimize the negative effects on the mechanical properties of the target material. Although the magnitude of the peak stresses caused by the proton beam impinging on the target may be considerably less than the yield stress of the material, failure due to material fatigue must be taken into consideration. The suitability of various tungsten alloys as target materials can be evaluated with a good knowledge of the fatigue properties of these alloys. However, a scan of literature indicates limited data reported for these alloys. Fracture toughness of tungsten heavy metal alloys has been studied by

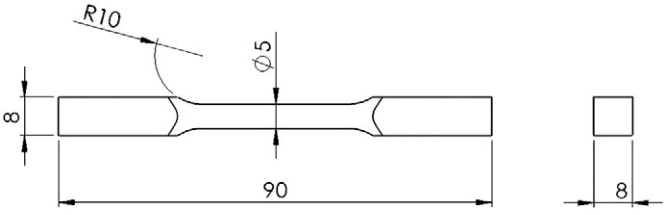

Fig. 1. Sample dimensions (in mm).

* Corresponding author.
E-mail addresses: srinivasan.iyengar@material.lth.se, srinivasan.iyengar@gmail.com (S. Iyengar).

0263-4368/$ – see front matter © 2013 Elsevier Ltd. All rights reserved.
http://dx.doi.org/10.1016/j.ijrmhm.2013.09.001

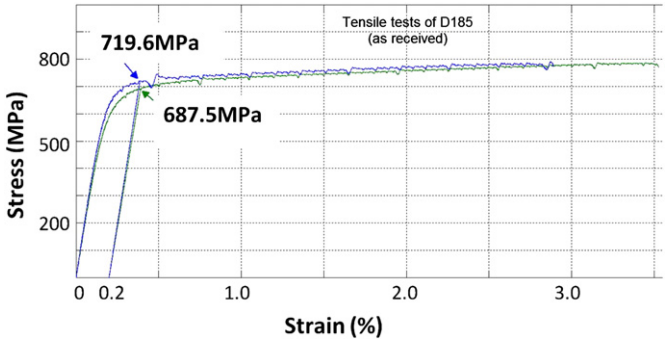

Fig. 2. Stress–strain curves for D185 alloy at 25 °C.

Table 1
Fatigue test data for D185 alloy at room temperature.

Specimen no.	σ_a (MPa)	N_f (10^5 cycles)	Specimen no.	σ_a (MPa)	N_f (10^5 cycles)
1	350	1.067	9	450	1.446
2	350	11.411	10, 11	250	Run-out[a]
3	350	2.459	11a	300	15.307
4	350	3.297	12	300	Run-out[a]
5	350	4.031	12a	350	3.803
6	350	Run-out[a]	13	400	1.046
7	450	4.720	14	300	Run-out[a]
8	450	2.740	14a	400	0.607

[a] Run-out: 2×10^6 cycles.

Zamora et al. [1]. They considered the effects of composition, grain size, prior plastic strain and the ductile phase surrounding the tungsten grains on fracture toughness. Rittel and Weisbrod [2] used a short beam experimental technique to characterize the mode I dynamic fracture toughness of a commercial tungsten heavy alloy (W–7 wt.% Ni–3 wt.% Fe) at loading rates of about 10^6 MPa $m^{1/2}$ s^{-1}. They found that the dynamic fracture toughness is rate sensitive and anisotropic. Ryu et al. [3] studied the microstructure and mechanical properties of a mechanically alloyed and solid-state sintered tungsten heavy alloy (W–5.6 wt.% Ni–1.4 wt.% Fe). For this alloy, they report an increase in yield strength due to the nanoscale microstructure, but reduced ductility due to the low volume fraction of the ductile phase present. Apart from these studies on fracture, not much data have been reported on the fatigue behavior of tungsten heavy alloys. Recently, Lorenzo et al. [4,5] studied the fatigue behavior of tungsten heavy alloys IT180 and D176 at room temperature. Along similar lines, the present study focuses on stress-controlled High Cycle Fatigue (HCF) experiments for the determination of fatigue properties and the establishment of a Stress–Life (S–N) curve for the tungsten heavy alloy Densimet 185 at room temperature.

2. Materials and methods

Seventeen specimens of the alloy Densimet 185 were supplied by Plansee and the specimen dimensions are shown in Fig. 1. After tensile testing, fatigue tests were conducted in the relatively high cycle fatigue region of 10^4 to 10^7 cycles, followed by microstructural characterization of the fracture surfaces.

An MTS Ramen machine (maximum capacity: 250kN) connected to an Instron Digital Electronic control system was used for tensile and fatigue testing (at zero mean stress). For metallographic examination using a Leitz optical microscope and an ESEM, the specimens were sectioned and mounted using a Predopress Struers machine. Fractographic studies and microstructural characterization were followed by Energy Dispersive Spectroscopy (EDS) and X-ray mapping.

3. Results and discussion

3.1. Mechanical testing

Two tensile tests on specimens (5.01 mm in diameter) in the as-received condition were carried out according to the ASTM practice E8 [6]. A gauge length of 12.5 mm was used and the loading rate was set to 3 mm/min until failure. The resulting stress–strain curves are shown in Fig. 2. Within the limits of experimental error, a small variation in the values of the Young's modulus and the 0.2% Proof stress were observed in the two sets of data.

Fifteen specimens were used for fatigue testing at various stress amplitudes in the interval 250 to 450 MPa, with 50 MPa increments and a mean stress equal to zero. A sinusoidal load with a frequency of 25 Hz was applied until specimen failure or up to the run-out limit which was considered to be 2×10^6 cycles.

Initially, three fatigue tests were performed using specimens in the as-received condition at a stress amplitude (σ_a) of 350 MPa. As seen in Table 1, for specimens 1 to 3, the test results showed a ten-fold variation in fatigue life from about 10^5 to 10^6 cycles. Further, all three specimens failed near the shoulder area. Examination of the surface roughness of the specimens revealed deviations from the ASTM standard [7]. In order to decrease the surface roughness, a grinding and polishing procedure was carried out prior to fatigue testing of the remaining specimens. Silicon carbide paper (320 and 1000 grains/in^2) and diamond paste (3 and 1 μm) were used for wet grinding/polishing of the specimens using a Struers Rotopol-2 equipment. Even after surface preparation, some striations from the specimen manufacturing stage were visible at a magnification 20×. Surface porosity was observed before and after the grinding/polishing operation. While some of the pores could be removed through grinding, sub-surface pores were visible after surface preparation. Fig. 3 shows the surface condition of Specimen 9, prior to and after polishing, at a magnification 25×. Surface roughness and the number of visible pores were observed to be more in the specimen shoulder region.

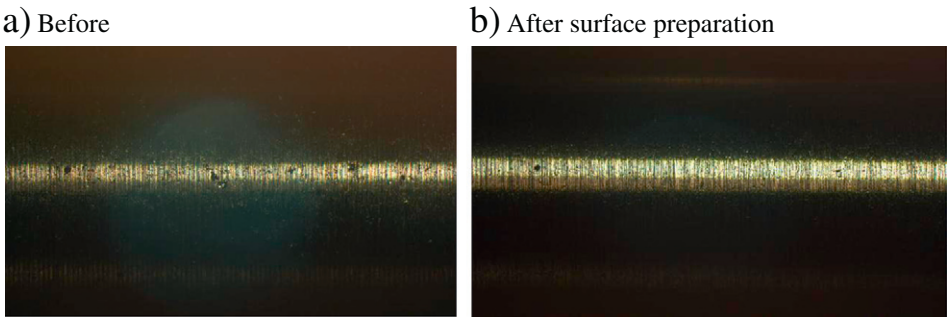

Fig. 3. Surface condition at the center (a) prior to and (b) after grinding and polishing (specimen 9, 25×).

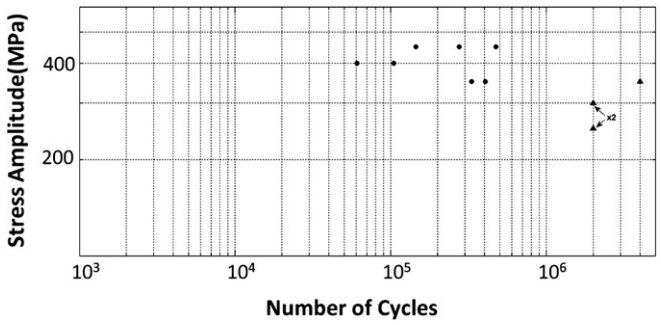

Fig. 4. *S–N* diagram for D185 alloy at room temperature (only polished specimens; ×2: two overlapping results).

Table 2
Mechanical properties and Basquin parameters.

Alloy	$R_{p0.2}$ [MPa]	E [GPa]	σ_e [MPa]	σ_f' [MPa]	b [−]	K_{Owen} [−]	$\sigma'_{f,Owen}$ [MPa]	s
D185	688–720	362–385	300	3550	−0.166	2.128	2230	0.59
D176	642	309	425	3000	−0.128	3.560	2553	0.153
IT180	612	208	210	1048	−0.112	2.727	868	0.268

The results from the fatigue tests are presented in Table 1 and Fig. 4. Fatigue data for specimens 1 to 3, tested in the as received condition, are not included in Fig. 4. Tests carried out at a stress amplitude of 350 MPa (specimens 4 to 6) showed a large variation in fatigue life (329,700 to 4×10^6 cycles). At 450 MPa (specimens 7 to 9), the variation in fatigue life was relatively small (144,600 to 472,000 cycles). Specimens 10 and 11 were tested at 250 MPa and survived 2×10^6 cycles. At 300 MPa, two run outs (specimens 12 and 14) and a failure at a relatively high fatigue life of 1.53×10^6 cycles (specimen 11a) were observed. Increasing the stress level to 400 MPa led to failures in specimens 13 and 14a. Specimens 11a and 14a refer to cases where run-out specimens at a lower stress level were subjected to higher stresses leading to failure. It may also be noted that three specimens (7, 8 and 15) failed close to the specimen shoulder, probably due to the surface roughness and the relatively small radius of curvature.

The material was assumed to follow a Basquin type of relation according to

$$\sigma_a = \sigma_f' \left(2N_f\right)^b$$

where σ_a is the stress amplitude, σ_f' the strength coefficient and b the strength exponent. Following the ASTM practice E739 [8] as outlined by Wirsching [9], a statistical analysis was made to get the best fit for the data in Table 1. The strength coefficient (σ_f') and the strength exponent (b) were determined to be 3550 MPa and −0.166 respectively.

Using Owen's one-sided tolerance limit according to the procedure of Lee et al. [10], a lower bound design curve was also determined. Although arbitrary, this choice was made because of the inherent advantages of being able to choose the reliability factor R and the confidence level C. Sample size is also baked into the concept. Using values of 90 and 95% for C and R, a 95% chance of survival with a 90% of confidence can be ensured for the fatigue life at a specified stress level. Assuming the strength exponent b to remain constant, the lower bound design *S–N* curve is obtained by shifting the estimated *S–N* curve to the left according to the equation:

$$\log N_{f,Owen} = \log N_f - K_{Owen} \times s$$

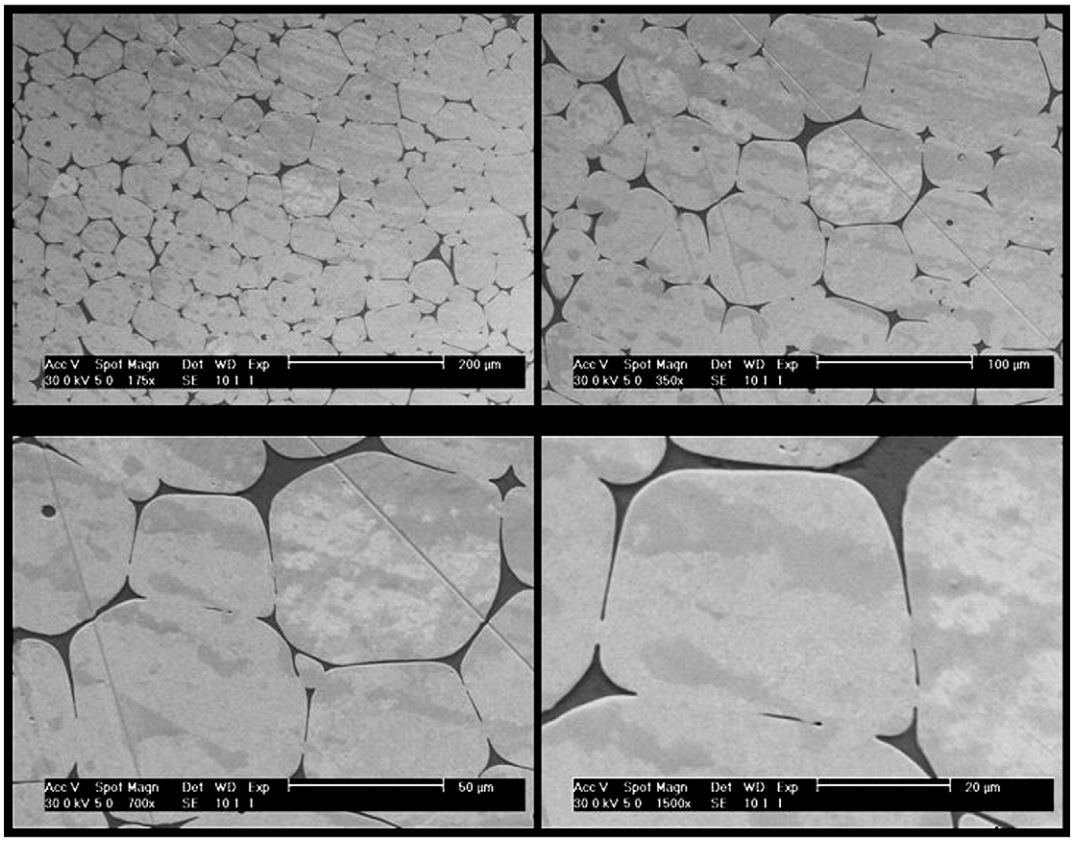

Fig. 5. SEM images of D185 alloy at different magnifications.

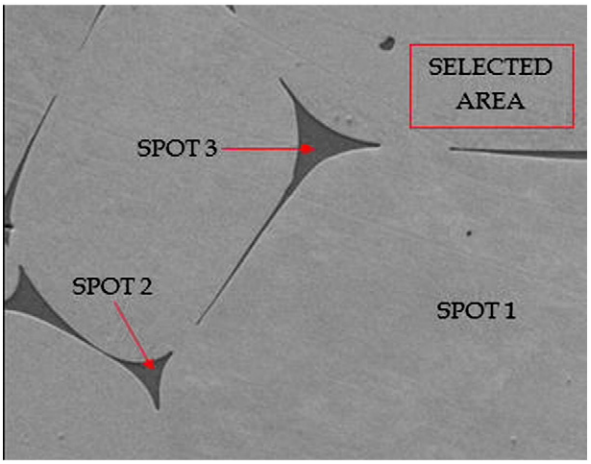

Fig. 6. Positions chosen for EDS analysis.

Table 3
EDS analysis showing the distribution of elements in the specimen.

Element	Spot 1	Spot 2	Spot 3	Selected area
W	99.2	28.76	36.51	98.97
Fe	0.33	21.06	20.12	0.41
Ni	0.47	50.19	43.37	0.62

Analyses in wt.%. The spots correspond to those shown in Fig. 6.

where K_{Owen} and s are the Owen-constant and standard deviation respectively. For the data in Table 1, K_{Owen} is 2.128 and the corresponding standard deviation is 0.59 which mirrors the scatter in experimental data.

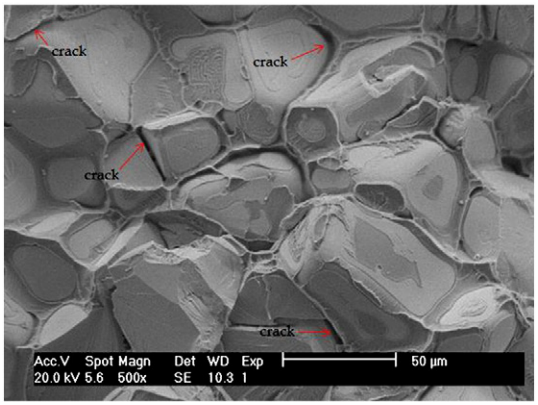

Fig. 8. SEM image of the fracture surface of a tensile test specimen.

After the shift, the Owen lower bound design curve can be expressed as:

$$\sigma_{a,Owen} = \sigma'_{f,Owen}\left(2N_{f,Owen}\right)^{b}.$$

In the present case, the strength coefficient ($\sigma'_{f,Owen}$) was evaluated to be 2230 MPa.

For purposes of comparison, Table 2 presents data on the mechanical properties and Basquin parameters for two other tungsten heavy alloys [1,2], D176 (W–5 wt.% Ni–2.5 wt.% Fe) and IT180 (W–3.5 wt.% Ni–1.5 wt.% Cu) together with those of D185. It is seen that D185 alloy has the highest Young's modulus among the alloys listed and its properties compare well with those of D176 alloy. The higher, uncompensated fatigue strength coefficient $\sigma'_{f,Owen}$ of D185 decreases below that of D176 after the Owen correction to $\sigma'_{f,Owen}$ due to the much higher standard

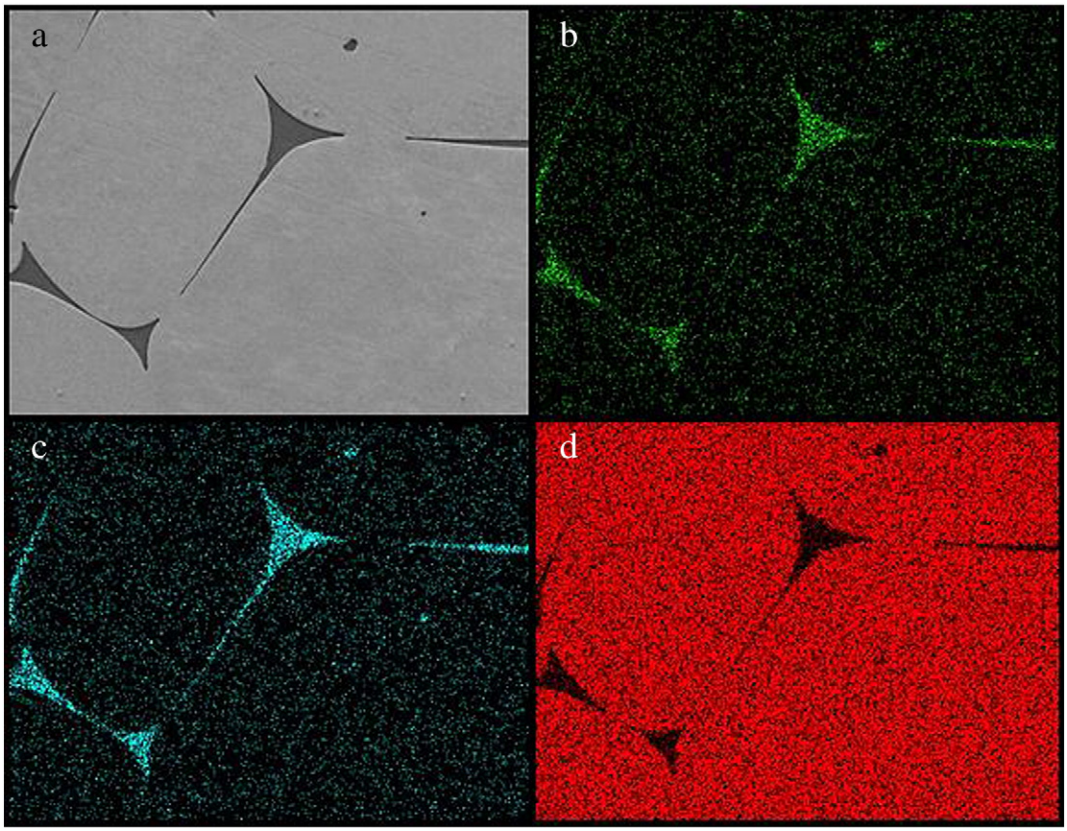

Fig. 7. Elemental mapping. (a) SEM image, (b) Fe-rich area (green), (c) Ni-rich area (blue) and (d) a W-rich area (red).

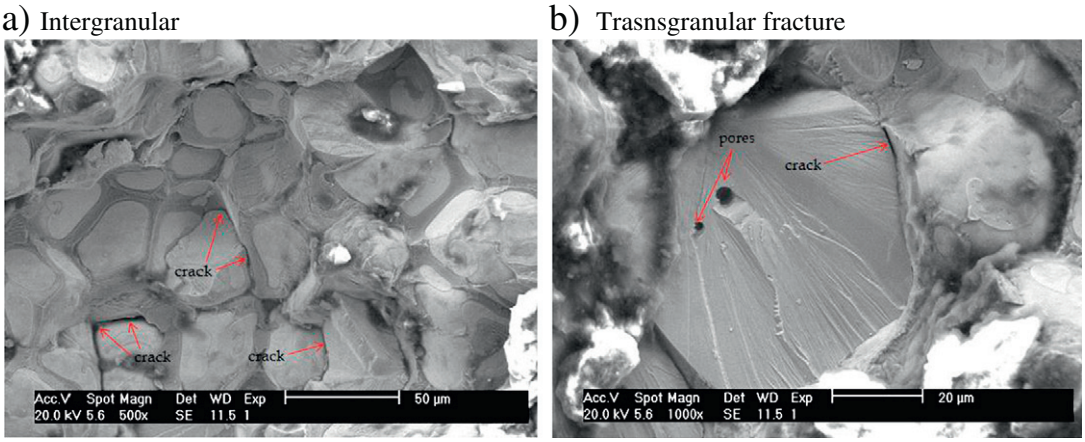

Fig. 9. SEM images of intergranular and transgranular fracture surfaces in specimen 8 after fatigue failure.

deviation (s) for D185. Also, the higher stiffness due to the strength exponent (b) decreases the capacity of D185 to accommodate fatigue loading relatively faster as compared to both D176 and IT180. Lower estimates of the endurance limit (σ_e) are also included in the following table.

3.2. Microstructural examination

D185 alloy specimens were ground and polished to get an even surface which was examined using an environmental scanning electron microscope. The images obtained at various magnifications are shown in Fig. 5. The tungsten grains are fairly rounded and the bonding phase appears to be uniformly distributed in the structure. The microstructure is also characterized by the direct bonding between the tungsten grains. Porosity in the specimen is low and indicative of a successful sintering process. The pores remaining in the specimen are mostly isolated in the tungsten grains and are clearly seen in the images.

3.3. Energy Dispersive Spectroscopy (EDS) and X-ray mapping

Fig. 6 shows the positions and the area selected for EDS analysis. The results are presented in Table 3.

3.4. Elemental mapping

In order to get a good idea about the distribution of various elements in the tungsten heavy alloy sample, X-ray mapping was carried out and the results are presented in Fig. 7. This confirms the presence of iron and nickel mostly in the ductile phase in between the tungsten grains.

3.5. Fractography

The fracture surface of one of the tensile test specimens was examined using the SEM and the image obtained is shown in Fig. 8. Intergranular fracture between tungsten spheroids (W–W) is clearly seen in the figure. This is the most frequently occurring fracture mode for tungsten alloys at room temperature.

Fig. 9 shows the images of the fracture surface of specimen 8 after fatigue failure. Both intergranular (W–W) and transgranular cleavages of tungsten spheroids (W) can be seen in these images. Cleavage is the principal fracture mechanism that requires the highest amount of energy and this might possibly explain why no such fracture was observed in the specimens that underwent tensile tests. Further, two pores which could have triggered the transgranular fracture can be clearly seen in the tungsten grain.

A fracture surface having pores within the tungsten grains as well as at the grain boundaries is shown in Fig. 10.

4. Conclusions

The fatigue failures observed at room temperature in the tungsten heavy alloy Densimet 185 were mostly of the intergranular type. A close examination of the microstructure revealed that this was due to inadequate bonding between tungsten grains in some areas. Porosity at the grain boundaries plays an important role and reduces the strength significantly. However, porosity levels can be controlled by optimizing sintering parameters like temperature, time, powder purity and particle size. A decrease in the size of pure tungsten particles would improve sintering kinetics and decrease the porosity in the sample. The primary requirement here is to achieve the required mechanical properties in the product while trying to keep the costs down. Care should also be taken to see that the final machining operations after sintering do not lead to rough surfaces with striations which aid fatigue crack nucleation. ASTM [7] has specified tolerance limits for surface roughness which can be used as a guide for finishing operations in the preparation of fatigue test samples. In this work, the endurance limit for the D185 alloy samples has been established to be in the range 300 to 350 MPa.

Acknowledgments

This work has been made possible due to the cooperation between ESS and the Division of Materials Engineering, LTH. We would like to thank Zivorad Zivkovic for his invaluable help in the laboratory.

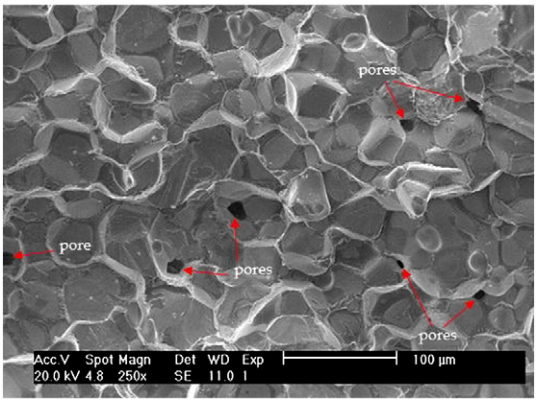

Fig. 10. Pores on the fracture surface.

References

[1] Zamara KMO, Sevillano JG JG, Pérez MF. Fracture toughness of W heavy metal alloys. Mater Sci Eng A 1992;157:151–60.
[2] Rittel D, Weisbrod G. Dynamic fracture of tungsten base heavy alloys. Int J Fract 2001;212:87–98.
[3] Ryu HJ, Hong SH, Baek WH. Microstructure and mechanical properties of mechanically alloyed and solid-state sintered tungsten heavy alloys. Mater Sci Eng A 2000;291:91–6.
[4] Lorenzo P, Miralda M, Iyengar S, Melin S, Noah E. Fatigue properties and characterization of tungsten heavy alloys IT180 & D176. Int J Refract Met Hard Mater 2013. http://dx.doi.org/10.1016/j.ijrmhm.2013.04.010.
[5] Lorenzo P, Miralda M. Fatigue properties of tungsten heavy alloys IT180 and D176. M.Sc. Thesis Sweden: Division of Materials Engineering, Lund University; June 2011.
[6] ASTM E8. Standard test methods for tension testing of metallic materials; 2000.
[7] ASTM E466-96. Standard practice for conducting force controlled constant amplitude axial fatigue tests of metallic materials; 2002.
[8] ASTM E739-91. Standard practice for statistical analysis of linear or linearized stress–life (*S*–*N*) and strain–life (*e*–*N*) fatigue data; 1998 (reapproved).
[9] Wirsching PH. Statistical summaries of fatigue data for design purposes; 1983 (NASA-CR-3697).
[10] Lee YL, Pan J, Hathaway RB, Barkey ME. Fatigue testing and analysis. London: Elsevier Butterworth-Heinemann; 2005.